Self-Detecting Mid-Infrared Dual-Comb Spectroscopy Based on High-Speed Injection-Locked Quantum Cascade Lasers

Yu Ma, Dapeng Wu, Ruixin Huang, Shichen Zhang, Binru Zhou, Zejun Ma, Yongqiang Sun, Junqi Liu, Ning Zhuo, Jinchuan Zhang, Shenqiang Zhai, Shuman Liu, Fengqi Liu, Manijeh Razeghi, and Quanyong Lu*

Dual-comb spectrometer based on quantum cascade lasers (QCLs) is gaining fast development and revolutionizing the precision measurement with high-frequency and temporal resolutions. In these measurements, high-bandwidth photodetectors are normally used for signal acquisition and processing, which complicates the measurement system. QCL is well-known for its picosecond gain-recovery time with an intrinsic bandwidth of tens of GHz. In this work, a compact self-detecting dual-comb spectroscopy (DCS) is demonstrated based on dispersion-engineered, high-speed packaged QCLs under coherent injection locking. The laser source is designed and fabricated into a hybrid-monolithic-integrated waveguide and epi-down packaged on a wideband-designed submount to fully explore the high-speed feature up to fourth-order harmonic state with a cutoff frequency of 40 GHz. The effective radio frequency (RF) injection locking diminishes the issue of optical feedback and enables high-bandwidth self-detection based on QCLs. Clear and stable multiheterodyne signal corresponding to a spectral range of 68 cm^{-1} and narrow comb tooth linewidth of ≈10 kHz is observed without using external detector or numerical process. The demonstrated broadband, high-power, self-detecting mid-infrared QCL DCS has a great potential for future applications of molecular sensing and spectroscopy.

1. Introduction

Optical frequency comb (OFC)[1] is a coherent laser source with equidistantly spaced comb lines and well-established phase relations. They act as optical rulers in frequency domain and have opened up a wide range of applications, including basic science, astrophysics, frequency metrology, communication, and precision spectroscopy.[2–4] Amidst these applications, dual-comb spectroscopy (DCS)[5,6] is the most widely used comb technology for its rapid effective data acquisitions without mechanical moving parts,[7,8] broad spectral coverage,[9–11] and high spectral resolution reaching comb line spacing of MHz.[10,12] The core configuration of DCS consists of two sets of OFCs with different repetition frequencies f_{rep} and their multiheterodyne beating in a fast detector to establish a one-to-one direct link from the optical frequency domain to the RF domain. The multiheterodyne generated comb in the RF domain enables a fast signal acquisition and process with higher resolution, speed, and precision performance that surpasses swept laser spectroscopy and Fourier transform spectroscopy.

The mid-infrared (mid-IR) region is of particular interest to molecular spectroscopic applications. A variety of molecules have peculiar molecular fingerprints with orders of magnitude higher absorption than those in the visible or near-IR bands due to their fundamental roto-vibrational absorption features in this range.[13–15] Quantum cascade lasers (QCLs)[16–18] has established themself as the leading laser source in mid-IR range thanks to the past three decades of persistent development and engineering. Owing to the large optical nonlinearity in the active region (AR), the dispersed longitudinal cavity modes can be locked to each other via the nonlinear process,[19–23] resulting

Y. Ma, S. Zhang, B. Zhou, Z. Ma, Q. Lu
Division of Quantum Materials and Devices
Beijing Academy of Quantum Information Sciences
Beijing, 100193, China
E-mail: luqy@baqis.ac.cn

The ORCID identification number(s) for the author(s) of this article can be found under https://doi.org/10.1002/adpr.202500062.

D. Wu, R. Huang, Y. Sun, J. Liu, N. Zhuo, J. Zhang, S. Zhai, S. Liu, F. Liu
Laboratory of Solid-State Optoelectronics Information Technology
Institute of Semiconductors, CAS
Beijing, 100049, China

M. Razeghi
Center for Quantum Devices
Department of Electrical Engineering and Computer Science
Northwestern University
Evanston, IL 60208, USA

ADVANCED
SCIENCE NEWS
www.advancedsciencenews.com

ADVANCED
PHOTONICS
RESEARCH
Open Access

www.adpr-journal.com

in the direct generation of phase-coherent frequency combs from QCLs. DCS based on QCL FCs[24–28] is enabling low-noise measurements with millisecond acquisition time and MHz spectral resolution.[5,29–31] Currently, most of the DCS systems based on free-running QCL FCs[31–35] rely on fast MCT detectors for multiheterodyne RF comb signal referencing and detecting, which increases the cost and complexity of the system. It is well known that QCL is a fast gain medium due to its sub-ps gain recovery time.[36] This could render QCL a broadband optical response when it is designed with a proper waveguide and packaging. However, the low-quality factor of the mid-IR Fabry–Pérot (FP) cavity makes the comb state rather susceptible to external optical feedback and optical isolator is normally used in comb characterization setup.[37,38]

The ultrafast characteristic of QCL with cutoff bandwidth of tens of GHz also suggests that the electronic beat signal at the repetition rate frequency f_{rep} can be observed through the feeding bias circuit and the cavity modes can be locked via RF modulation at f_{rep} via the same process.[15,20,39,40] Actually, RF injection locking at the round-trip frequency is being demonstrated as an effective way to lock f_{rep} and enhance the robustness of the comb mode. Nevertheless, it requires a specialized waveguide for efficient RF signal injection.[41,42] To fully explore this ultrafast feature, various high-speed waveguide and packaging techniques have been proposed and implemented.[42–44] In the THz range, the metal–metal waveguide of THz QCL is ideal

to achieve high RF bandwidth,[45,46] while in the mid-IR range, QCL has been fabricated into microstrip waveguide, and the RF signal is then injected to a short section of the laser cavity device for efficient RF signal injection.[42,44,47,48] However, most of present high-speed results are achieved at the price of output power by shrinking the device active and thermal contact areas. The present microstrip-waveguide design, featuring a narrow metal waveguide stripe to reduce the parasitic capacitance for wide bandwidth response, however, is not quite compatible to epi-down mounting scheme that is essential to high-power operation at room temperature.

In this work, we report a hybrid-monolithic-integration waveguide (HMIWG) structure with a high-speed packaging for self-detecting mid-IR QCL DCS at $\lambda \approx 4.6\,\mu m$ with a high output power, broad spectral coverage, and strong comb coherence, as shown in **Figure 1**a. A segregated-coplanar waveguide (CPW) together with a monolithic-multimode-coupled waveguide structure is designed and fabricated for RF injection and group velocity dispersion (GVD) engineering. A broadband RF bandwidth up to 40 GHz and effective RF injection locking up to the third-order harmonic state is observed from a 4.5-mm-long dispersion-engineered QCL comb at 4.6 μm. This broadband feature enables the QCL comb serving a high-bandwidth photodetector in the DCS system without the use of external detectors. Stable multiheterodyne signal with a broad RF comb bandwidth of 1.4 GHz and a narrow tooth linewidth ≈10 kHz is observed,
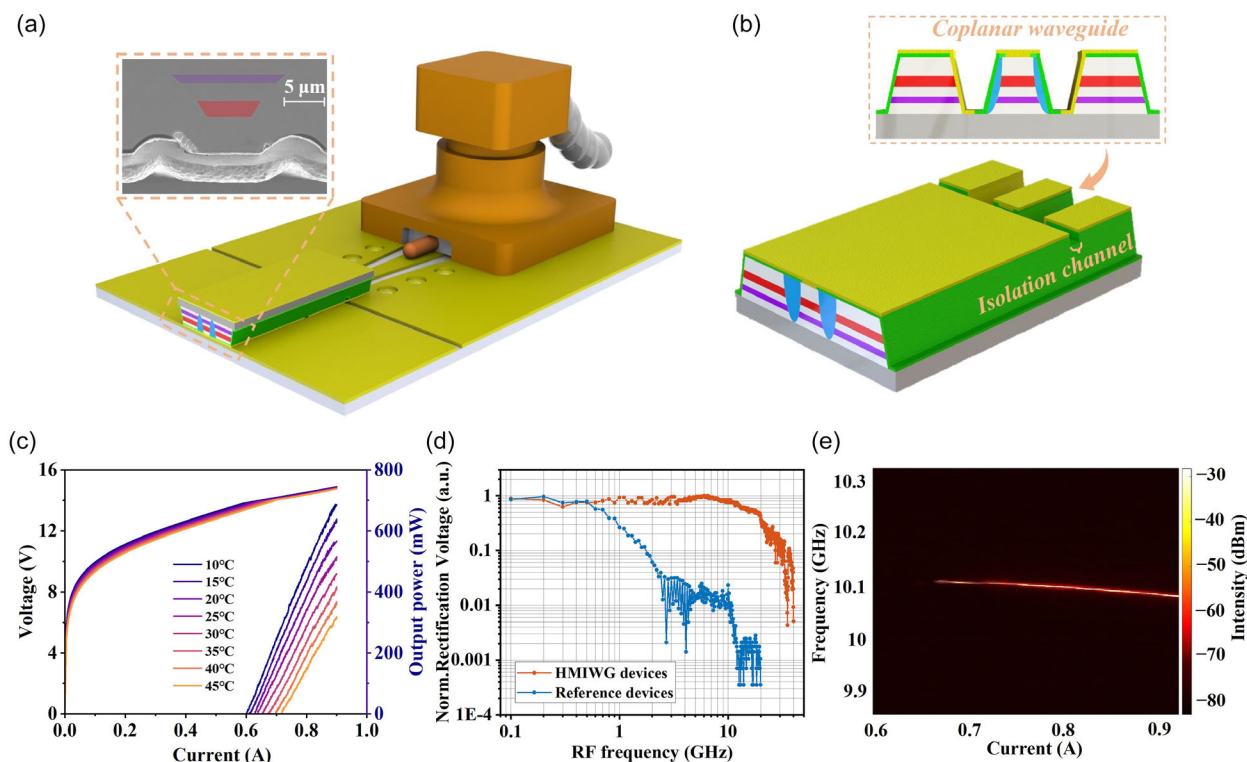
Figure 1. High-speed design and characterizations for HMIWG QCLs. a) Schematic diagram of devices based on a hybrid-monolithic-integration waveguide structure with high-speed packaging. Inset: false-colored scanning electron microscopy image (SEM) of the front facet of a device. b) Schematic diagram of a segregated-CPW structure. c) L–I–V characterization of a 4.5-mm-long high reflective coated device in continuous-wave (CW) operation at 10−45 °C. d) Normalized electrical rectification data of the HMIWG device and that of a reference device without high-speed packaging. e) Free running beatnote mapping as a function of drive current measured at 15 °C in CW mode. RBW is set as 300 kHz and VBW is 3 kHz.

corresponding to a broad optical spectrum 68 cm^{-1} at 4.6 μm. This self-detecting DCS scheme simplifies the experimental setup for currently used DCS system but with an enhanced spectral bandwidth and signal-to-noise ratio (SNR), paving the way for new spectroscopy applications based on QCL DCS with improved heterodyne–comb linewidth and reduced system complexity.

2. Results

Recent studies on the OFC operation of QCL using coupled-mode formalism based on Maxwell–Bloch equations revealed that both the GVD and RF modulation play important roles in the comb dynamics (Section S1, Supporting Information). Toward this end, the HMIWG device is designed with an effective dispersion compensation as well as coherent RF injection scheme to obtain a comb light source with wide spectrum, high power, and strong coherence, which provides a reliable architecture for the self-detecting DCS. For mid-wave 3–5 μm QCLs with strong material GVDs, without effective dispersion engineering, the RF injection locking range would be hampered.[47] The dispersion compensation in this work is achieved via a multimode-coupled waveguide structure shown in Figure 1a. A passive InGaAs waveguide layer is sandwiched between the AR and substrate and is naturally integrated into the waveguide when a deep-etch and planarization regrowth processing is performed for dispersion compensation. The spacer thickness between the active and passive waveguides is judicious engineered to ensure sufficient GVD dispersion and confinement factor of the AR, as the details presented in Section S2, Supporting Information.
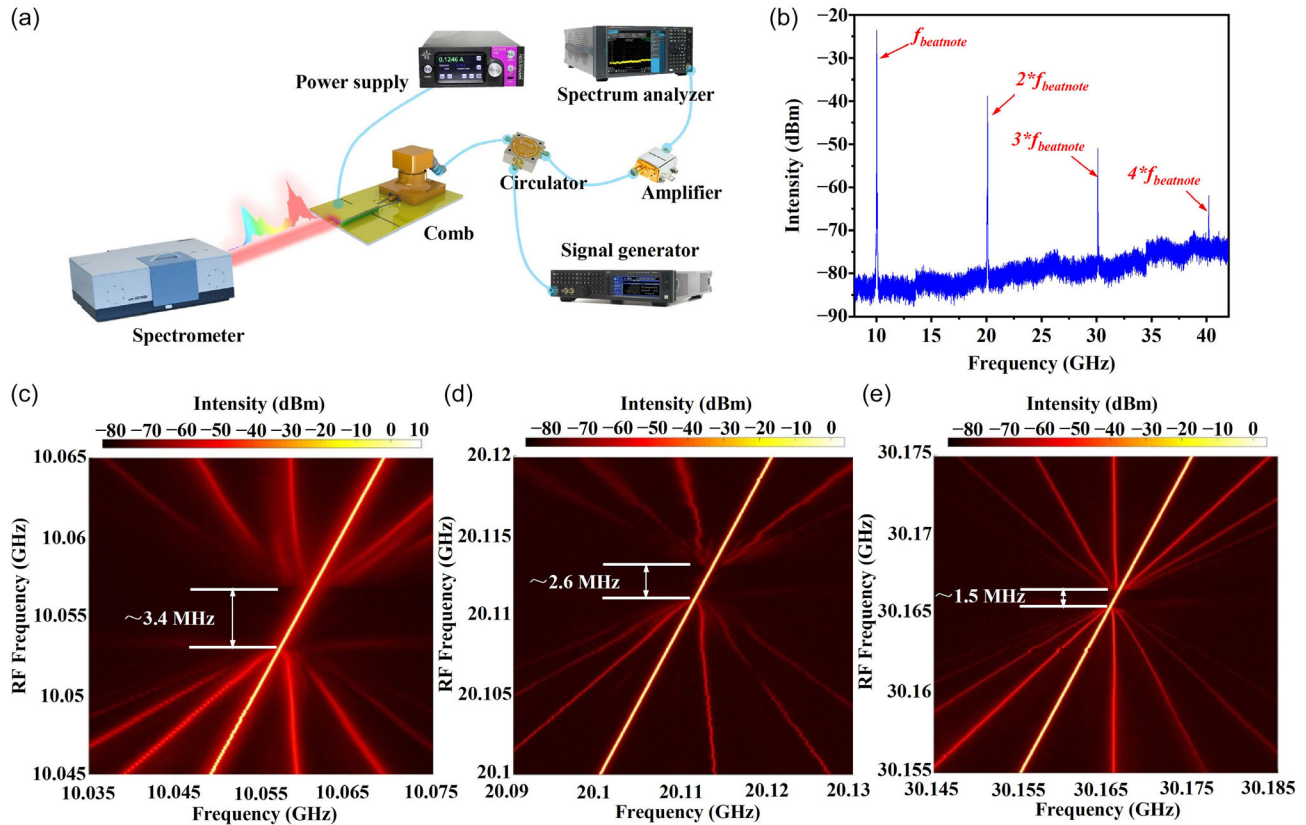
Upon the dispersion-engineered waveguide, a segregated-coplanar section with high-speed packaging is designed and fabricated at the cavity end to achieve effective RF injection. It is electrically isolated with the rest of the waveguide section via an etched channel into the cladding layer and the rest of the device via two etched trenches into the substrate. The two auxiliary waveguides on the two sides act as the bonding pads for epi-down process. The channel is defined into 1.5 μm deep and 50 μm wide with an equivalent resistance of 2 kΩ for electrical isolation while still remaining optically transparent, as shown in the simulation in Figure S5b, Supporting Information. As indicated in Section S3, Supporting Information, the −3 dB bandwidth of conventional devices is mainly affected by the bypass section capacitance C_{bypass}, and the cutoff frequency of the device is mainly affected by the gold wire inductance L_{gold} and the heat sink parasitic capacitance C_{hs} outside the QCL chip. Here, the segregated CPW section is electrically isolated with the rest to largely reduce C_{bypass}, as shown in Figure 1b. The length of this section is limited to about 1/10 of the cavity to further reduce the parasitic capacitance as well as to provide efficient RF extraction and injection. Its DC bias can be adjusted to alter the locking properties. The device was epi-down bonded to a wideband CPW predefined on a AlN submount. The RF signal is fed or extracted through a mini SMP that is directed soldered to the submount, avoiding any poor contact when attaching an RF probe to the device. This is advantageous in reducing the impact of the gold wire inductance L_{gold}. In contrast to conventional packaging structures, hollow-plated vias passing through the submount were arranged near the end of the device to connect the ground traces on the top to the ground and thus to reduce the heat sink parasitic capacitance C_{hs}. This high-speed epi-down mounting scheme is crucial to high power and high bandwidth response of the QCL comb.

Light–current–voltage (L–I–V) characterizations (Figure 1c) for the HMIWG device with high-speed packaging were performed while driving the device in CW by a power supply (Wavelength Electronics, QCL2000) at heat sink temperatures in the range of 10–45 °C. The device was installed on a water-cooling platform using a thermoelectric cooler (TEC) for temperature control. A thermistor was closely connected to these components for real-time temperature adjustment. The emitted optical power was measured with a calibrated thermopile detector placed in front of the laser facet without any correction. At 10 °C, a 6.5-μm-wide and 4.5-mm-long device exhibited a maximum CW output power about 700 mW and a threshold current density of 2.05 kA cm^{-2}.

For the high-frequency characterization, the HMIWG device was biased with a direct current (DC) together with a microwave signal modulation to measure the electrical bandwidth using a microwave rectification technique. A conventional FP device is also tested for comparison. Figure 1d shows the normalized electrical rectification signal of the two devices, measured at a constant RF power of 10 dBm. The −3 dB bandwidth of the segregated CPW device was 16.2 and 0.7 GHz for the conventional epi-down-bonded device. More importantly, the cutoff frequency at −15 dB for the two devices are 40 and 3 GHz, respectively. The observed −3 dB bandwidth and the cutoff frequency at −15 dB for the HMIWG device are comparable to those of the state-of-the-art microstrip waveguide design.[42] It is evident that the HMIWG device preserves the high-power feature at room temperature, thanks to the improved thermal dissipation, while also endued with a high-speed characteristic, comparable to other designs.[27,28] Narrow intermode beatnote signal is observed at 0.67 A and persists continuously until 0.92 A, over 80% of the dynamic range, as shown in Figure 1e. This is attributed to the well dispersion-engineered multimode-coupled waveguide design.[49] The spectra were acquired using a spectrum analyzer (Keysight N9030B) with a resolution bandwidth (RBW) of 300 kHz and video bandwidth (VBW) of 3 kHz at 300 K.

The high bandwidth feature not only facilitate the injection locking of the fundamental comb state with 1 FSR, but it also opens the door to the effective injection locking of the higher harmonic states with multiple FSRs. Since a broadband QCL comb consists of plethora of equally spaced longitudinal modes, the beatnote is the joint result of the electrical beating between any two longitudinal modes. We set up the test system as shown in **Figure 2**a and the following measurements in **Figure** 2 and **3** used the same testing run conditions to provide the best correlation of the data. When zoomed out the beatnote at $I = 0.882$ A, the first-order beatnote at ≈10.05 GHz together with higher-harmonic-state beating signals at ≈20.10, 30.15, and 40.20 GHz was observed, thanks to the wideband waveguide design and high-speed packing, as shown in Figure 2b. Clearly, harmonic, especially high-order harmonic states are inherent to QCLs and their injection locking is of great importance for future high-power, high-speed applications and would open new approach

**ADVANCED
SCIENCE NEWS**

www.advancedsciencenews.com

**ADVANCED
PHOTONICS
RESEARCH**
Open Access

www.adpr-journal.com

Figure 2. Fundamental and higher harmonic-state injection locking for HMIWG QCLs. a) The experimental setup for RF-injection-locking measurement, including spectrum analyzer (KEYSIGHT, N9030B, 2 Hz–44 GHz), signal generator (KEYSIGHT N5183B, from 9 kHz to 40 GHz, 15 dBm, or Rohde & Schwarz SMF100A, 22 GHz, 30 dBm), Fourier transform infrared spectrometer (Bruker VERTEX 70v), circulator (UIYBCC1325A), power supply (Wavelength Electronics, QCL2000). b) Fundamental, second-harmonic, third-harmonic, and fourth-harmonic beatnotes at an injection current of 0.882 A. Electronic RF spectra of RF modulation as functions of frequencies near three different beatnote frequencies: c) $f_{RF} \approx f_{beatnote}$; d) $f_{RF} \approx 2*f_{beatnote}$; and e) $f_{RF} \approx 3*f_{beatnote}$, respectively.

to the mode-locking of QCLs with high peak power and wide spectral range.[44,49]

Recent findings revealed that the beatnote of a QCL comb can be injection-locked to an external RF oscillator while maintaining full intermodal coherence. This enables all-electric stabilization similarly to phase-locked loops with increased comb spectral range and enhanced robustness against optical feedback. Under an injection current of 0.882 A, the frequency of the RF signal applied to the device is tuned around the beatnotes to evaluate the evolution of the injection locking. Figure 2a shows the testing setup, including temperature control, power supply, amplifier, RF circulator, signal generator, and high-frequency connection cables. Figure 2c–e exhibits the measured beatnote spectra while sweeping the injection frequency across the beatnote at the first three harmonic-state frequencies. As the frequency of the injected signal approaches the beatnote frequency, a frequency pulling effect is observed.[42,45] This is a nonlinear mixing effect between the external injected RF beatnote and the internal electrical beatnote directly generated from the AR. Therefore, a broadband packaging is the key in the observation of this frequency pulling effect. The comb beatnotes are fully controlled by the external RF oscillator within a locking range

$\Delta f_{lock} \propto \frac{\kappa f_{beatnote}}{2\pi^2}\sqrt{\frac{I_{RF}}{I_{cavity}}}$. Here, κ is a factor related to the quality factor of the free running oscillator resonator. The resonant locking range of $f_{RF} \approx f_{beatnote}$, $f_{RF} \approx 2*f_{beatnote}$, and $f_{RF} \approx 3*f_{beatnote}$, are respectively 3.4, 2.6, and 1.5 MHz. Due to the different injection efficiency at different frequencies (Figure 3b), the locking bandwidth decreases with the increase of frequency under the same power RF injection (f_{RF} = 15 dBm). While the injection locking of the fundamental beatnote has been extensively studied, no clear demonstrations have been realised on higher-order harmonic beatnote, especially above the third-order states. The injection-locking of higher-order states is of particular interest in high-bit-rate optical communication, photonic analogue-to-digital conversion, multiphoton imaging, and astronomical frequency comb generation.[44]

The coherent injection locking is further verified by comparing the emission spectra of QCLs with and without RF modulations. Figure 3a,c shows the evolution of the spectral distributions with the RF modulation power and RF modulation frequency. When RF signal is in resonance with the fundamental beatnote frequency of the device, a nearly flat center and prominent side band excitation with an extended spectral coverage from 40 to 75 cm^{-1} is observed under a DC bias of 0.882 A
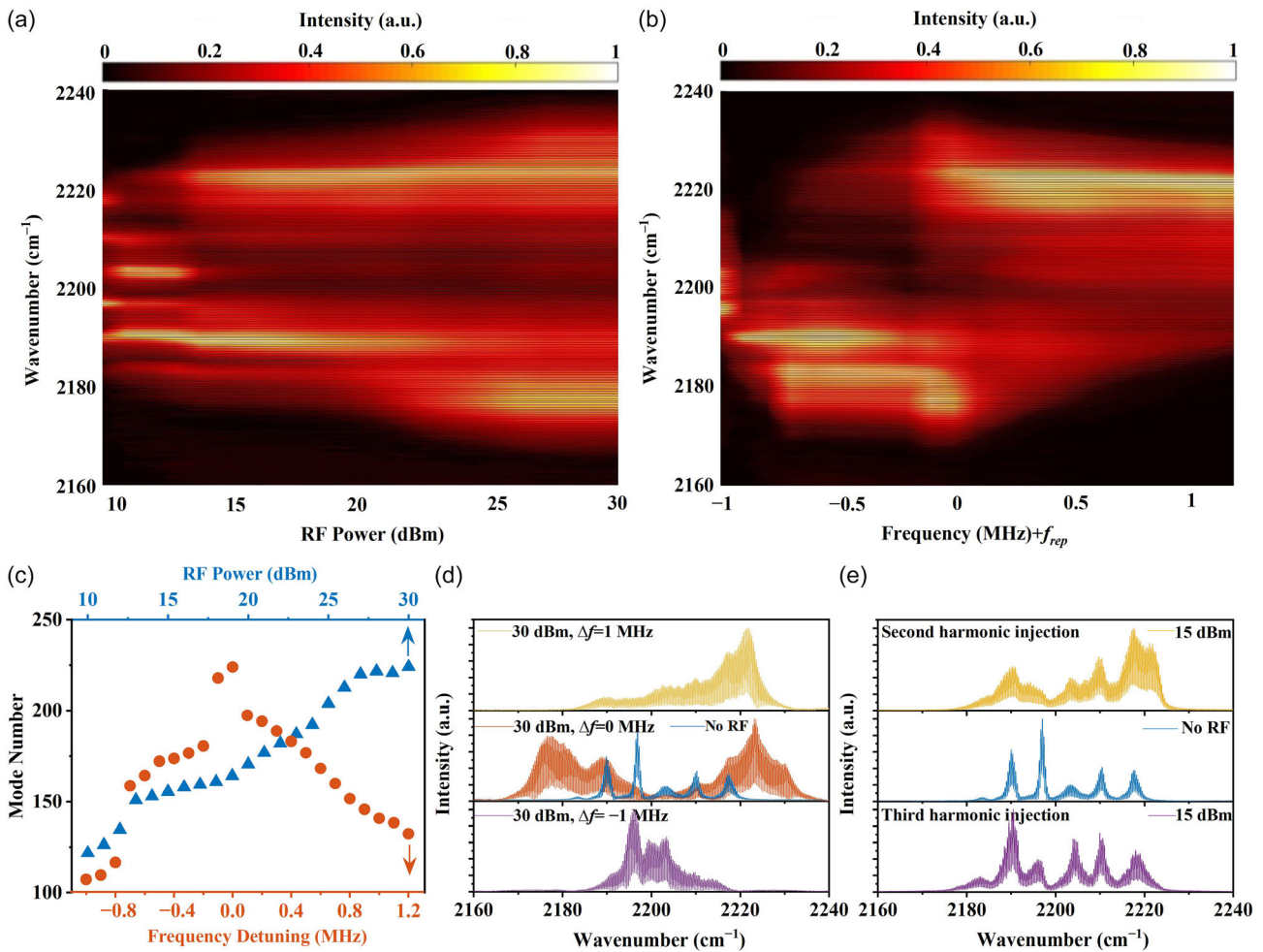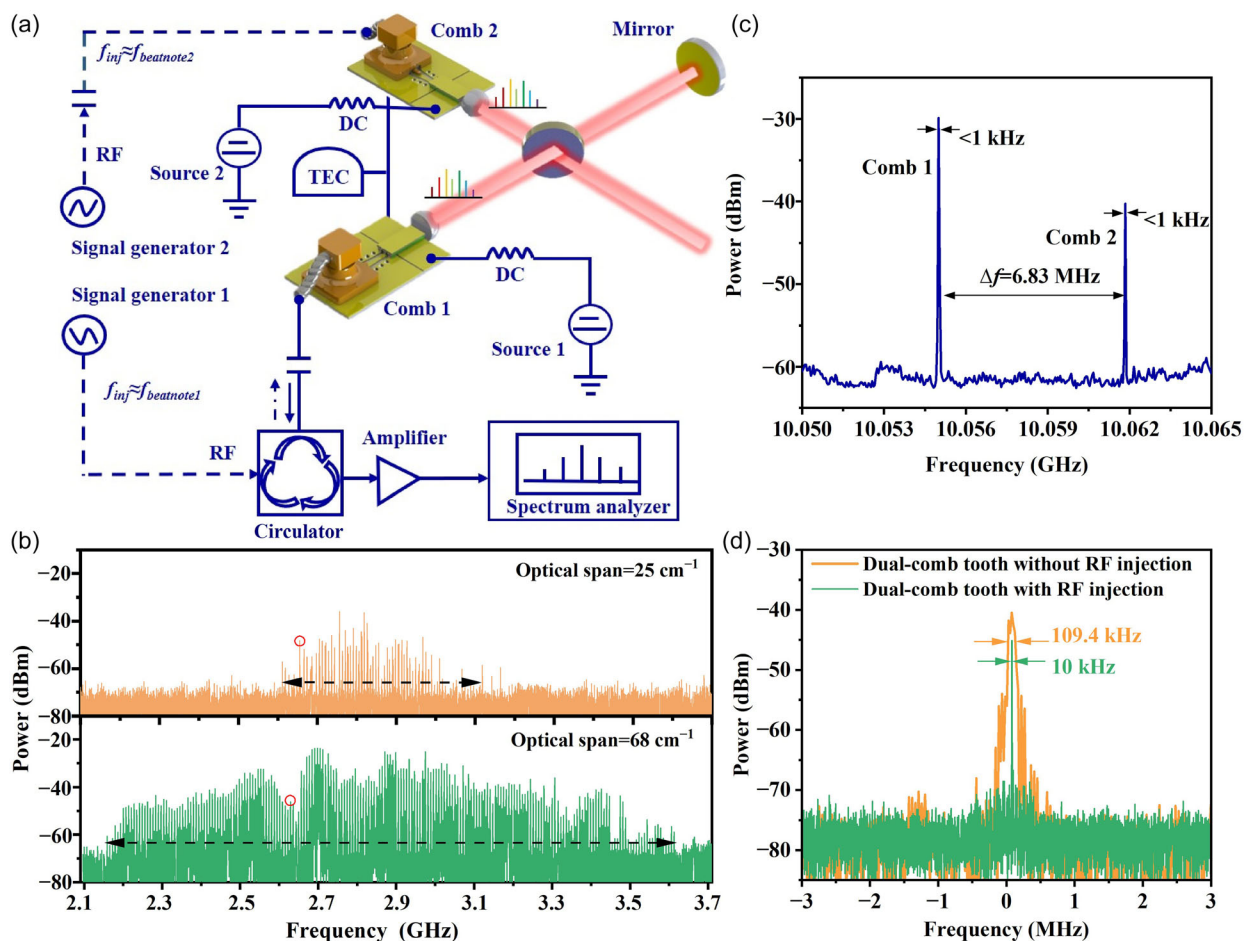
Figure 3. Spectral characterizations for HMIWG QCLs under various RF modulation conditions. a) Spectral sweeping under different RF injection power at $\Delta f = 0$ MHz. b) Spectra for sweeps of the RF injection frequency at RF power = 30 dBm. c) Mode number as a function of the injection power when $\Delta f = 0$ MHz and injection frequency at RF power = 30 dBm, respectively. d) Spectral characterizations at RF power = 30 dBm under different frequency detuning $\Delta f = 1, 0, -1$ MHz, respectively, and compared that with no RF injection. e) Spectral characterizations of second-harmonic injection and third-harmonic injection at RF power = 15 dBm and $\Delta f = 0$ MHz, respectively, and comparison with no RF injection.

and 30 dBm RF modulation. A new distribution of the spectral intensities among the modes is clearly visible. When the RF signal is tuned away from the beatnote yet still within the locking range (≈ 3.4 MHz), spectral broadening is also be obtained, but the broadening effect is reduced and spectral imbalance is observed, as shown in Figure 3b,c. Therefore, the spectral bandwidth of QCL comb is shown to be continuously tunable by varying the RF injection frequency or power (Figure 3d). In a similar fashion, we also record the emission spectra of the device with and without RF modulation when RF modulation is in resonance with second-harmonic or third-harmonic beatnote in Figure 3e. Clear spectral broadening and intensity redistribution for both cases are observed under a DC bias of 0.882 A and 15 dBm RF modulation.

For a FP QCL, the spectral bandwidth is influenced by multiple factors, including gain, GVD, Kerr nonlinearity, etc.[37] The external RF modulation near the round-trip frequency, however, requires no redesign of the laser quantum structure and can

vastly tune the spectra bandwidth within the locking range, as demonstrated earlier. Due to the dependence of the locking range with the injected power, the optimization of the injection efficiency is crucial to broadening of the spectrum. In a low-dispersion-engineered cavity, the new excited side bands under external microwave modulation would exhibit a comblike operation with a fixed interval between modes. It has been shown that the comb state inside a QCL is quite sensitive to optical feedback and optical isolator or neutral density filter is normally used to reduce this feedback.[37,38,49] Under coherent RF injection locking,[25] QCL comb has shown the enhanced robustness despite of optical feedback. In this work, the wideband HMIWG and high-speed packaging further transform the injection-locked QCL into a high-speed photodetector which is ideal for self-detection of dual multiheterodyne spectroscopy to verify the comb operation.

Figure 4a is the schematic of a mid-IR self-detecting DCS based on injection-locked high-speed GVD-engineered QCLs at $\lambda \approx 4.6\,\mu$m. The two laser beams are collimated first and

**ADVANCED
SCIENCE NEWS**

www.advancedsciencenews.com

**ADVANCED
PHOTONICS
RESEARCH**

www.adpr-journal.com

Figure 4. Self-detecting DCS based on injection-locked HMIWG QCLs. a) Experimental setup for self-detecting DCS system based on injection-locked QCLs. b) Multiheterodyne spectra (real-time acquisition) of the two combs without RF injection and with RF injection. RBW: 510 kHz, acquisition time: ≈3.35 ms. c) Beatnotes of the Comb 1 and Comb 2 measured with a spectra analyzer, both linewidths of two combs are less than 1 kHz. d) A typical dual-comb tooth under RF injection (green line, corresponding to the red circle in Figure 4b) with a FWHM of ≈10 kHz, and a typical dual-comb tooth without RF injection (orange line, corresponding to the red circle in Figure 4b) with an FWHM of 109.4 kHz. The corresponding RBWs are 7.5 and 75 kHz, respectively.

recombined using a ZnSe-coated beam splitter. A reflecting mirror is placed at the one of combined laser beam for light feedback into the wideband HMIWG devices for multiheterodyne spectroscopy. One of the devices, Comb 1, is used as a fast detector for recording the multiheterodyne beating signals by exploiting its fast intersubband relaxation process and the intrinsic nonlinearities in the AR. The two devices are biased at currents of 0.882 and 0.780 A, respectively, and installed on the same water-cooling platform with TEC at 15 °C to suppress the inter temperature drifting. Figure 4c shows the intermode beatnotes extracted via a horn antenna (A-INFO-LB-28-10-C-KF) placed at the vicinity to the lasers. The linewidths of beatnotes for the two combs are both less than 1 kHz and their frequency spacing is tuned to 6.83 MHz. Strong coherence between the modes is indicated by the narrow linewidths of the intermode beatnotes, which can be used to monitor the state of the comb operation during data acquisition. The multiheterodyne signal is extracted via the RF modulation feeding line from Comb 1 and real-time recorded using a spectrum analyzer (KEYSIGHT, N9030B, 2 Hz–44 GHz).

Compared with the numerical processed double-comb multiheterodyne signal in the literature,[24,31] the real-time observation method is more convincing and convenient. The dual-comb multiheterodyne spectrum of the two combs under RF injection exhibits a coverage of ≈1.4 GHz containing a total ≈200 comb lines, as seen in the lower panel of Figure 4b. This corresponds to a spectrum spanning of 68 cm^{-1}, which matches well with the spectral overlap range under RF injection (75 cm^{-1}) and demonstrates that the devices operate as frequency combs on the whole spectral bandwidth. When the RF injection source on Comb 2 is turned off, the self-detecting dual-comb multiheterodyne bandwidth shrinks to 25 cm^{-1} and the RF signal becomes unstable and instantaneous owing to the optical feedback to the unlocked comb device. The full-width at half-maximum (FWHM) of a dual-comb tooth without RF injection is 109.4 kHz. Under RF injection, the FWHM of a dual-comb tooth is significantly reduced to ≈10 kHz. This is about two-order of magnitude lower than that of unlocked dual-comb heterodyne tooth linewidth using an external photodetector.[50] The clear dual-comb teeth with

**ADVANCED
SCIENCE NEWS**

www.advancedsciencenews.com

**ADVANCED
PHOTONICS
RESEARCH**

www.adpr-journal.com

reduced linewidth prove the devices operate under injection-locked comb states well-defined phase relation among different modes. Note that the comb lines of the multiheterodyne spectrum from the injection-locked self-detecting QCL DCS exhibits enhanced SNRs of 25–40 dB. This is compared to SNRs of $\approx$10–25 dB from DCS system without RF injection shown in the upper panel of Figure 4b or free running cases in refs. [49,50]. The enhanced SNRs here is attributed to the stabilization feature of the RF injection locking technique. At the same time, the obvious broadening of the dual-comb heterodyne RF spectra under RF injection is clearly attributed to the enhanced spectral bandwidth enabled by the RF modulation. Compared with the dual-comb system without RF injection locking,[51] the present self-detection system under injection locking can withstand strong optical feedback up to $\approx$10% of the emitted power from each device. The two collimated and combined beams possess much stronger beam spatial intensity and thus is advantageous in detecting highly absorbing matters. The last but not the least, the current self-detecting DCS system doesn't require the use of external detectors as well as numerical processing of the RF heterodyne signal, therefore, can be easily adapted into a DCS for sensing spectroscopy application with a much compact format and reduced system complexity (see Supporting Information).

3. Conclusion

Self-detecting DCS without external detectors is highly desired and would significantly simplify the present DCS system. QCL comb with intrinsic bandwidth up to tens of GHz is ideal for high-speed photodetection. This makes it possible for self-detection. However, self-detecting DCS in the mid-IR frequency range has yet to be demonstrated with similar spectral bandwidth and robustness to those if the DCS using external detectors. In this work, we demonstrated a compact self-detecting DCS system based on dispersion-engineered QCLs under high-speed packaging and coherent RF injection locking. The HMIWG device is fabricated to obtain a comb light source at $\lambda \approx 4.6\,\mu m$ with wide spectrum, high power, and strong coherence, which provides a reliable support for the self-detecting DCS. Harmonic states up to fourth order at 40.20 GHz is observed from a free-running QCL comb. Meanwhile, coherent RF injection up to the third-order harmonic state and clear spectral broadening are achieved, demonstrating the high-speed feature of the device design and packaging. Coherent RF injection locking enable QCL comb withstanding strong optical feedback and make it ideal for dual-comb self-detection. Broad multiheterodyne signal corresponding to 68 cm^{-1} spectral coverage and narrow dual-comb tooth $\approx$10 kHz is recorded from the self-detecting DCS system, which show the unique advantages in intermode coherence, high-power output, spectral broadening, and system simplification. In the future, we will use a stable external frequency source to stabilize the comb frequency and further enhance the system resolution for future spectroscopy application.[52] In conclusion, the use of dispersion engineering, high-speed packaging, and RF injection provides all the necessary features for DCS and will lead to monolithic-integrated DCS where optical feedback is inevitable and could be properly addressed under the presented high-speed injection-locking scheme. The features of high power,

wide spectrum, narrow RF comb linewidth, and simple format would further promote mid-IR DCS from fundamental research to wide range application.

4. Experimental Section

The QCL comb wafer was grown by metal-organic chemical vapor deposition (MOCVD) using the InGaAs/AlInAs material system on an n-InP:Si ($2 \times 10^{18}\,cm^{-3}$) substrate. The template preparation starts with a InP buffer layer ($2 \times 10^{18}\,cm^{-3}$), a 1.2 μm thick InGaAs passive waveguide, and a 1.6 μm thick InP spacing layer. The doping level of the spacing layer grades from 5×10^{16} to $1 \times 10^{17}\,cm^{-3}$ during growth target the desired evanescent coupling. After a 40-stage single-core AR growth placed between two 100 nm thin layers of InGaAs ($2 \times 10^{16}\,cm^{-3}$), the top cladding layers were then grown. The top cladding layers sequence is 3 μm thick InP cladding layer ($2 \times 10^{16}\,cm^{-3}$) and 0.5 μm thick InP contact layer ($5 \times 10^{18}\,cm^{-3}$). Ridge widths of 6.5 and 12 μm for the AR and passive waveguides were targeted in the wet-etching fabrication process prior to the lateral InP:Fe-insulating layer was grown by MOCVD. Finally, the segregated CPW was dry-etched using SiO$_2$ as the hard mask to reduce the inherent parasitic capacitance. The device was then bonded to a wideband CPW transition on AlN substrate which was used as an interposer connection between mini SMP cables and QCL.

All of the 2D simulations were carried out by using COMSOL Multiphysics 6.1. A module of electromagnetic waves, frequency domain under the catalog of optics, was utilized to simulate the optical modes for various geometries of the HMIWG device.

Supporting Information

Supporting Information is available from the Wiley Online Library or from the author.

Conflict of Interest

The authors declare no conflict of interest.

Author Contributions

Yu Ma: conceptualization (equal); data curation (lead); formal analysis (equal); investigation (lead); writing—original draft (equal); writing—review & editing (equal). **Dapeng Wu**: investigation (equal). **Ruixin Huang**: investigation (equal). **Shichen Zhang**: investigation (supporting). **Binru Zhou**: investigation (supporting). **Zejun Ma**: investigation (supporting). **Yongqiang Sun**: investigation (supporting). **Junqi Liu**: investigation (supporting). **Ning Zhuo**: investigation (supporting). **Jinchuan Zhang**: investigation (supporting). **Shenqiang Zhai**: investigation (supporting). **Shuman Liu**: funding acquisition (equal); investigation (equal). **Fengqi Liu**: funding acquisition (lead); resources (equal); writing—review & editing (equal). **Manijeh Razeghi**: investigation (equal); writing—review &

[1] T. Udem, R. Holzwarth, T. W. Hänsch, *Nature* **2002**, *416*, 233.

[2] P. Trocha, M. Karpov, D. Ganin, M. H. Pfeiffer, A. Kordts, S. Wolf, J. Krockenberger, P. Marin-Palomo, C. Weimann, S. Randel, W. Freude, T. J. Kippenberg, C. Koos, *Science* **2018**, *359*, 887.

[3] T. Fortier, E. Baumann, *Commun. Phys.* **2019**, *2*, 153.

[4] P. Martín-Mateos, F. U. Khan, O. E. Bonilla-Manrique, *Optica* **2020**, *7*, 199.

[5] I. Coddington, N. Newbury, W. Swann, *Optica* **2016**, *3*, 414.

[6] E. Vicentini, Z. Wang, K. Van Gasse, T. W. Hänsch, N. Picqué, *Nat. Photonics* **2021**, *15*, 890.

[7] T. Ideguchi, S. Holzner, B. Bernhardt, G. Guelachvili, N. Picqué, T. W. Hänsch, *Nature* **2013**, *502*, 355.

[8] L. Zhou, X. Qin, Y. F. Di, H. P. Lou, J. P. Zhang, Z. J. Deng, C. L. Gu, D. P. Luo, W. X. Li, *Opt. Lett.* **2023**, *48*, 4673.

[9] A. V. Muraviev, V. O. Smolski, Z. E. Loparo, K. L. Vodopyanov, *Nat. Photonics* **2018**, *12*, 209.

[10] Z. Chen, M. Yan, T. W. Hänsch, N. Picqué, *Nat. Commun.* **2018**, *9*, 3035.

[11] G. Ycas, F. R. Giorgetta, E. Baumann, I. Coddington, D. Herman, S. A. Diddams, N. R. Newbury, *Nat. Photonics* **2018**, *12*, 202.

[12] I. Coddington, W. C. Swann, N. R. Newbury, *Phys. Rev. Lett.* **2008**, *100*, 013902.

[13] L. Consolino, M. Nafa, M. De Regis, F. Cappelli, K. Garrasi, F. P. Mezzapesa, L. Li, A. G. Davies, E. H. Linfield, M. S. Vitiello, S. Bartalini, P. De Natale, *Commun. Phys.* **2020**, *3*, 69.

[14] B. Jerez, P. Martín-Mateos, E. Prior, C. De Dios, P. Acedo, *Opt. Express* **2016**, *24*, 14986.

[15] M. Razeghi, Q. Lu, D. Wu, S. Slivken, in *Proc. SPIE 10756, Terahertz Emitters, Receivers, and Applications IX*, San Diego, CA, September **2018**, p. 107560I.

[16] M. Razeghi, Q. Y. Lu, N. Bandyopadhyay, W. Zhou, D. Heydari, Y. Bai, S. Slivken, *Opt. Express* **2015**, *23*, 8462.

[17] J. Faist, F. Capasso, D. L. Sivco, C. Sirtori, A. L. Hutchinson, A. Y. Cho, *Science* **1994**, *264*, 553.

[18] Q. Lu, S. Slivken, D. Wu, M. Razeghi, *Opt. Express* **2020**, *28*, 15181.

[19] A. Hugi, G. Villares, S. Blaser, H. C. Liu, J. Faist, *Nature* **2012**, *492*, 229.

[20] L. Consolino, F. Cappelli, M. S. De Cumis, P. De Natale, *Nanophotonics* **2019**, *8*, 181.

[21] Q. Y. Lu, M. Razeghi, S. Slivken, N. Bandyopadhyay, Y. Bai, W. J. Zhou, M. Chen, D. Heydari, A. Haddadi, R. McClintock, M. Amanti, C. Sirtori, *Appl. Phys. Lett.* **2015**, *106*, 051105.

[22] Y. Yang, D. Burghoff, D. J. Hayton, J. R. Gao, J. L. Reno, Q. Hu, *Optica* **2016**, *3*, 499.

[23] P. Tzenov, D. Burghoff, Q. Hu, C. Jirauschek, *IEEE Trans. Terahertz Sci. Technol.* **2017**, *7*, 351.

[24] G. Villares, A. Hugi, S. Blaser, J. Faist, *Nat. Commun.* **2014**, *5*, 5192.

[25] J. Hillbrand, A. M. Andrews, H. Detz, G. Strasser, B. Schwarz, *Nat. Photonics* **2019**, *13*, 101.

[26] J. B. Khurgin, Y. Dikmelik, A. Hugi, J. Faist, *Appl. Phys. Lett.* **2014**, *104*, 081118.

[27] S. Hakobyan, R. Maulini, S. Blaser, T. Gresch, A. Muller, *Opt. Express* **2020**, *28*, 20714.

[28] R. Wang, P. Täschler, F. Kapsalidis, M. Shahmohammadi, M. Beck, J. Faist, *Opt. Lett.* **2020**, *45*, 6462.

[29] P. Jouy, J. M. Wolf, Y. Bidaux, P. Allmendinger, M. Mangold, M. Beck, J. Faist, *Appl. Phys. Lett.* **2017**, *111*, 141102.

[30] G. Villares, J. Wolf, D. Kazakov, M. J. Süess, A. Hugi, M. Beck, J. Faist, *Appl. Phys. Lett.* **2015**, *107*, 251104.

[31] J. Westberg, L. A. Sterczewski, F. Kapsalidis, Y. Bidaux, J. M. Wolf, M. Beck, J. Faist, G. Wysocki, *Opt. Lett.* **2018**, *43*, 4522.

[32] L. A. Sterczewski, J. Westberg, Y. Yang, D. Burghoff, J. Reno, Q. Hu, G. Wysocki, *Optica* **2019**, *6*, 766.

[33] N. Corrias, T. Gabbrielli, P. De Natale, L. Consolino, F. Cappelli, *Opt. Express* **2022**, *30*, 10217.

[34] Q. Lu, F. Wang, D. Wu, S. Slivken, M. Razeghi, *Nat. Commun.* **2019**, *10*, 2403.

[35] Y. Yang, D. Burghoff, J. Reno, Q. Hu, *Opt. Lett.* **2017**, *42*, 3888.

[36] Q. Lu, D. Wu, S. Slivken, M. Razeghi, *Sci. Rep.* **2017**, *7*, 43806.

[37] M. Piccardo, P. Chevalier, T. S. Mansuripur, D. Kazakov, Y. Wang, N. A. Rubin, L. Meadowcroft, A. Belyanin, F. Capasso, *Opt. Express* **2018**, *26*, 9464.

[38] M. Singleton, P. Jouy, M. Beck, J. Faist, *Optica* **2018**, *5*, 948.

[39] J. Hillbrand, N. Opačak, M. Piccardo, H. Schneider, G. Strasser, F. Capasso, B. Schwarz, *Nat. Commun.* **2020**, *11*, 5788.

[40] B. Schneider, F. Kapsalidis, M. Bertrand, M. Singleton, J. Hillbrand, M. Beck, J. Faist, *Laser Photonics Rev.* **2021**, *15*, 2100242.

[41] G. Villares, J. Faist, *Opt. Express* **2015**, *23*, 1651.

[42] F. Kapsalidis, B. Schneider, M. Singleton, M. Bertrand, E. Gini, M. Beck, J. Faist, *Appl. Phys. Lett.* **2021**, *118*, 071101.

[43] Y. Ma, X. Gao, W. Li, N. Liu, N. Zhuo, K. Yang, J. C. Zhang, S. Q. Zhai, S. M. Liu, L. J. Wang, F. Q. Liu, *Opt. Express* **2023**, *31*, 9729.

[44] F. Wang, S. Slivken, M. Razeghi, *Photonics Res.* **2021**, *9*, 1078.

[45] A. Forrer, M. Franckié, D. Stark, T. Olariu, M. Beck, J. Faist, G. Scalari, *ACS Photonics* **2020**, *7*, 784.

[46] A. Forrer, L. Bosco, M. Beck, J. Faist, G. Scalari, *Photonics* **2020**, *7*, 9.

[47] E. Rodriguez, A. Mottaghizadeh, D. Gacemi, M. Jeannin, Z. Asghari, A. Vasanelli, Y. Todorov, Q. J. Wang, C. Sirtori, *Laser Photonics Rev.* **2020**, *14*, 1900389.

[48] A. Calvar, M. I. Amanti, M. Renaudat St-Jean, S. Barbieri, A. Bismuto, E. Gini, M. Beck, J. Faist, C. Sirtori, *Appl. Phys. Lett.* **2013**, *102*, 181114.

[49] D. P. Wu, Y. Ma, Y. Q. Sun, R. X. Huang, J. C. Zhang, S. M. Liu, S. Q. Zhai, F. M. Cheng, F. Q. Liu, Q. Y. Lu, *Photonics Res.* **2024**, *12*, 2566.

[50] Y. Bidaux, F. Kapsalidis, P. Jouy, M. Beck, J. Faist, *Laser Photonics Rev.* **2018**, *12*, 1700323.

[51] H. Li, Z. Li, W. Wan, K. Zhou, X. Liao, S. Yang, C. Wang, J. Cao, H. Zeng, *ACS Photonics* **2019**, *7*, 49.

[52] K. N. Komagata, V. J. Wittwer, T. Südmeyer, L. Emmenegger, M. Gianella, *Phys. Rev. Res.* **2023**, *5*, 013047.